

Journal of Biomedical Optics

SPIEDigitalLibrary.org/jbo

Optimized goniometer for determination of the scattering phase function of suspended particles: simulations and measurements

Florian Foschum
Alwin Kienle

Optimized goniometer for determination of the scattering phase function of suspended particles: simulations and measurements

Florian Foschum and Alwin Kienle

Institut für Lasertechnologien in der Medizin und Meßtechnik an der Universität Ulm, Helmholtzstr 12, 89081 Ulm, Germany

Abstract. We present simulations and measurements with an optimized goniometer for determination of the scattering phase function of suspended particles. We applied the Monte Carlo method, using a radially layered cylindrical geometry and mismatched boundary conditions, in order to investigate the influence of reflections caused by the interfaces of the glass cuvette and the scatterer concentration on the accurate determination of the scattering phase function. Based on these simulations we built an apparatus which allows direct measurement of the phase function from $\vartheta = 7^\circ$ to $\vartheta = 172^\circ$ without any need for correction algorithms. Goniometric measurements on polystyrene and SiO₂ spheres proved this concept. Using the validated goniometer, we measured the phase function of yeast cells, demonstrating the improvement of the new system compared to standard goniometers. Furthermore, the scattering phase function of different fat emulsions, like Intralipid, was determined precisely.

© 2013 Society of Photo-Optical Instrumentation Engineers (SPIE) [DOI: [10.1117/1.JBO.18.8.085002](https://doi.org/10.1117/1.JBO.18.8.085002)]

Keywords: goniometer; static light scattering; scattering phase function; multiple scattering; Intralipid; yeast.

Paper 130285R received Apr. 26, 2013; revised manuscript received Jun. 5, 2013; accepted for publication Jun. 7, 2013; published online Aug. 23, 2013.

1 Introduction

Light distribution in biological tissue is usually described by the radiative transfer theory. This theory is based on the following optical properties of the investigated medium. Besides the refractive index n , the absorption coefficient μ_a , and the scattering coefficient μ_s , the phase function $p(\vartheta)$ ^{1,2} is used for the optical characterization of the medium. Often, a standard phase function is applied as phase function (e.g., the Henyey–Greenstein function³). However, for an exact description of the light propagation, the precise scattering phase function is needed. For ideal spherical scatterers, this function can be calculated using Mie theory,⁴ an analytical solution of Maxwell's equations. However, for arbitrary shaped particles or for an arrangement of spheres with unknown size distribution, it is very time-consuming or even not possible to calculate the phase function, although different numerical solutions of Maxwell's equations are available. Therefore, it is very important to have the possibility to measure the phase function of suspended particles.⁵ For these measurements, an apparatus called goniometer is frequently used.

In corresponding literature, several articles dealing with measurements of the scattering phase function can be found.^{6–13} Furthermore, a variety of articles dealing with the application of goniometric setups for biological and technical scatterers^{14–21} show the importance of precise measurements. Although a lot of work has been done in that field, there are still some unsatisfying issues to be addressed. For the calculation of the anisotropy factor, one needs to measure the largest possible angular range. For a lot of the cited apparatus, the

accessible angular range is limited. Especially, angles larger than $\vartheta \approx 140^\circ$ were often not accessible. Furthermore, the comparison of measured scattering phase functions of ideal spherical scatterers with Mie theory was often not satisfying, especially for strong forward scatterers. As far as the authors know, there is no publication dealing with the simulation of the light propagation in a cylindrical scattering cell applied for goniometric measurements. With the use of such a simulation, effects of reflections and multiple scattering can be examined. For media with an aligned microstructure, 2-axis goniometers have been developed.^{22,23} However, this is not the target of this publication, which actually addresses symmetrical or randomly oriented suspended particles.

In this work, we present a Monte Carlo method for the light propagation in a goniometric setup. Using this method, a frequently applied geometry is studied. Based on these simulations, an optimized apparatus is designed. The comparison of measurements on polystyrene and SiO₂ spheres with Mie theory proves the concept of the presented goniometer. With the improved goniometer, the scattering phase function of fat emulsions, like Intralipid, were determined. In a biological application using yeast cells, the need of measuring the broad angular range is demonstrated. The improvement of the optimized setup is shown through measurements of the scattering phase function determined with an improved cuvette, compared to those of a standard cuvette.

2 Monte Carlo Simulation

For better understanding and optimization of the goniometric measurement results, a Monte Carlo-based method for the light propagation in a cylindrical cuvette was implemented.

Address all correspondence to: Institut für Lasertechnologien in der Medizin und Meßtechnik an der Universität Ulm, Helmholtzstr 12, 89081 Ulm, Germany. Tel: ++49 (0)731/1429-779; Fax: +49 (0)731/1429-442; E-mail: florian.foschum@ilm.uni-ulm.de

The Monte Carlo method is within its stochastic nature an exact solution of the radiative transfer theory.²⁴ A Monte Carlo code for a radially n -layered cylindrical geometry of finite height with mismatched boundary conditions was developed. Hence, these simulations include, e.g., all reflections of the incoming and the scattered light at the cuvette interfaces. We started with a simulation of a possible setup, using a cylindrical cuvette ($\varnothing = 40$ mm, $n = 1.46$) filled with a suspension of polystyrene spheres ($\varnothing = 2.75$ μm , $\mu_s = 0.04$ mm^{-1} , unpolarized light) in water ($n = 1.33$). The cuvette was illuminated with a collimated beam ($\varnothing = 3$ mm) through the cylindrical face in direction to the center of the cuvette. The scattered photons around the cuvette were detected by a moveable point detector (distance to center 200 mm, resolution 1 deg). The resulting signal and the original phase function are shown in Fig. 1.

The detected signal differs strongly from the original phase function. This can be explained by the following effects. Due to the differences in refractive index of the medium ($n = 1.33$), the cuvette ($n = 1.46$), and the surrounding air ($n = 1$), there are reflections on each interface. The reflection on the first two interfaces of the incoming beam (air-glass and glass-medium) causes a back-reflection of $\sim 3.5\%$. As the cuvette is round, the reflection is angularly broadened up to 9 deg. Therefore, it is not possible to measure the phase function for angles larger than 171 deg. Furthermore, the reflections on the last two interfaces (medium-glass and glass-air) cause the photons to travel in the opposite direction, with a probability of again $\sim 3.5\%$. These photons can, in addition, be scattered by the polystyrene spheres. The measured signal is, therefore, the original phase function, superposed with 3.5% of the same phase function in the opposite direction (180 deg $-\vartheta$). This causes the increase of the signal, especially for angles > 130 deg and a smearing of the small oscillations, see Fig. 1. Another object to address is the method of detection. By using a point detector without imaging optics, we collect photons from any location of the illuminated sample volume. Together with the refraction at the transition from the scattering medium into the surrounding medium, this causes a smearing of the small oscillations of the phase function.

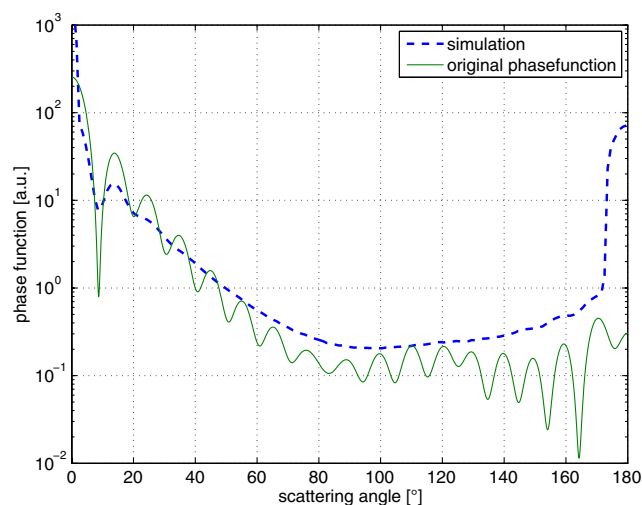


Fig. 1 Simulation of the detected signal of a possible goniometer compared to the original phase function of polystyrene spheres ($\varnothing = 2.75$ μm , $\mu_s = 0.04$ mm^{-1} , unpolarized light).

2.1 Improved Apparatus

In order to avoid these problems, we simulated an improved setup, as shown in Fig. 2. To minimize the effect of the broadened back-reflection on the entrance of the cuvette, we used a flat entrance window in the simulation. In addition, we applied a rather large cuvette of $\varnothing = 50$ mm (inner diameter: $\varnothing = 45$ mm), made of Schott Borofloat glass ($n_{635\text{nm}} = 1.46$), and a narrow incident collimated beam of $\varnothing = 2$ mm. The inner surface of the cuvette in the simulation is coated by a black absorbing layer, reaching from $\vartheta = -175$ deg to $\vartheta = 5$ deg with respect to the incident beam (see Fig. 2). Using this layer, we avoided transmission of the specular reflection through the medium in the opposite direction. For realization of this layer in the real measurement, see Sec. 3.

In the simulation, the scattered photons were detected analogously to a possible detection setup. In order to collect just photons scattered within a small solid angle, they were detected by imaging the origin of the cuvette onto the entrance surface of an optical fiber by using a lens (see Fig. 2). With an additional iris in front of the imaging lens, only photons scattered within an approximately cylindrical volume in direction to the iris were detected. The detection geometry was implemented in the Monte Carlo simulation by modeling the iris ($\varnothing = 3$ mm), the refraction at the lens ($f = 50$ mm, 3:1 magnification), and a detection surface, using a diameter of the detection fiber of 1 mm. Applying a diameter of 3 mm of the iris leads to an angular resolution of ~ 2 deg. This size of aperture is needed to collect enough light. The overlap of the illuminated and the cylindrical detection volumes decreases for detection angles from 0 deg to 90 deg, and increases again to 180 deg, see Fig. 2. This can be considered by

$$p(\vartheta) = m(\vartheta) \sin(\vartheta), \quad (1)$$

as long as the detection volume does not overlap the side faces of the cylindrical illumination volume ($\vartheta > 5$ deg and $\vartheta < 175$ deg). In Eq. (1), $p(\vartheta)$ is the corrected scattering phase function and $m(\vartheta)$ is the measured intensity. The validity of the formula was checked by using a CAD program.

In Fig. 3, simulations with this setup are shown for polystyrene spheres of 2.75 μm diameter (unpolarized light) and the Henyey-Greenstein phase function with $g = 0.8$. The scattering coefficient was set to be $\mu_s = 0.01$ mm^{-1} . The results for the Henyey-Greenstein phase function are multiplied by a factor of 10 for a better visualization. For the angular range between

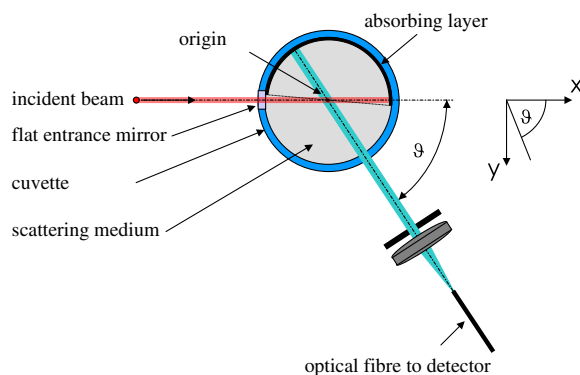


Fig. 2 Scheme of the improved goniometric setup, applied in the Monte Carlo simulation, showing the absorbing layer and the detection geometry.

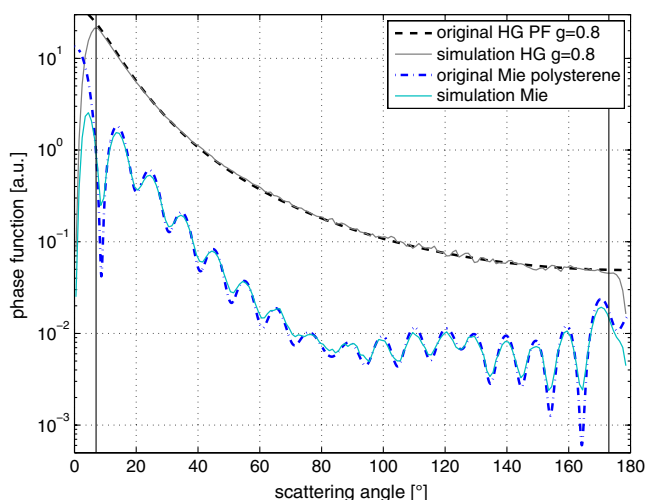


Fig. 3 Simulation of the detected signal from the improved setup in comparison with the original phase function. Simulations with a Henyey–Greenstein (HG) and a Mie phase function for $2.75\ \mu\text{m}$ polystyrene spheres (Mie) are shown.

$\vartheta = 7\ \text{deg}$ and $\vartheta = 173\ \text{deg}$, the simulations fit the original phase functions well. The angular resolution of $2\ \text{deg}$ flattens the small oscillations of the Mie phase function slightly. This is not a problem for the smooth Henyey–Greenstein phase function. For angles smaller than $\vartheta = 7\ \text{deg}$, the detected signal drops down, as the absorbing layer enters the detection path. For angles above $\vartheta = 173\ \text{deg}$, the detection volume overlaps the side face of the illumination volume, which causes also a decrease of the detected signal. In real measurements, this effect is replaced by the effect that the border of the flat entrance window enters the detection path. This causes a disturbance of the phase function for angles larger than $\vartheta = 172\ \text{deg}$. These two angular regions, therefore, cannot be measured and have to be extrapolated if needed.

2.2 Concentration of the Scatterers

Using the described Monte Carlo method, we investigated the influence of the scatterer concentration on the determination of the scattering phase function. If the concentration is too high, multiple scattering occurs, and the measurement of the phase function is disturbed. On the other hand, the intensity of the detected light decreases with reduced concentration of the scatterers. In Fig. 4, we present simulations with a sequentially varied scattering coefficient between $\mu_s = 0.1\ \text{mm}^{-1}$ and $\mu_s = 0.005\ \text{mm}^{-1}$. The scattering phase functions are normalized by using the integral in the angular region from $\vartheta = 20\ \text{deg}$ to $\vartheta = 160\ \text{deg}$. For a scattering coefficient of $\mu_s = 0.1\ \text{mm}^{-1}$, the simulated scattering phase function differs clearly from the original phase function. The simulation results improve by decreasing the concentration of the scatterers. For a scattering coefficient $\mu_s \leq 0.01\ \text{mm}^{-1}$, the simulated phase function shows no further deviations, besides the already discussed smearing of the small oscillations. For measurements of unknown particles we suggest to measure μ_s , using, e.g., a collimated transmission setup, and to dilute the suspension to produce samples with a scattering coefficient of $\mu_s = 0.01\ \text{mm}^{-1}$.

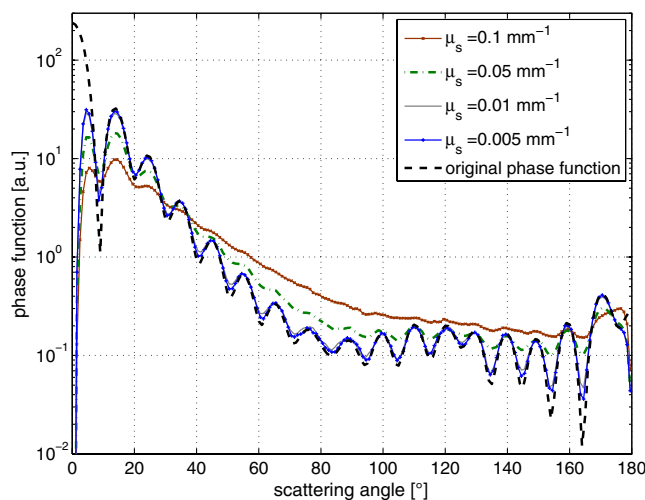


Fig. 4 Influence of the scatterer concentration and the multiple scattering on the determination of the scattering phase function.

3 Measurement System

Using the information obtained from these simulations, we built the goniometer shown in Fig. 5. We decided to fix the illumination together with the cuvette directly onto the shaft of a stepper motor (Mdrive 23 plus, Schneider Electric Motion USA, Marlborough), and turn it relative to the fixed detection unit. This avoids changes in the bending radius of the optical fiber used for detection. The illumination path is shown in Fig. 5(b). We used a $635\ \text{nm}/60\ \text{mW}$ laser diode (LDT-635-60G-TTL, TOPAG Lasertechnik GmbH, Darmstadt, Germany) with removed optics. The standard deviation of the power of this laser diode was determined to be $<1\%$ within a measurement interval of $10\ \text{min}$ (after $15\ \text{min}$ warmup). The diverging beam of the laser diode was focused by means of two lenses ($f = 20\ \text{mm}$ and $f = 60\ \text{mm}$) into a $200\ \mu\text{m}$ pinhole, used for beam shaping. The resultant diverging beam was then collimated by another $20\ \text{mm}$ lens. The following iris of $\varnothing = 2\ \text{mm}$ shapes the beam, which was then reflected $90\ \text{deg}$ by a mirror, mounted in order that the measurement field of view is not blocked (compare Fig. 5). A linear polarizer was used to produce well-defined polarized light. By turning the laser diode and the linear polarizer, the polarization was adjusted parallel or perpendicular with respect to the scattering plane. The sample was illuminated with a light power of $\approx 25\ \text{mW}$. For realization of the absorbing layer, the rear part of the cuvette was made of black anodized aluminum. For improvement of the absorption properties, the aluminum was sandblasted before anodization. A flat entrance window and a cylindrical cuvette window ($\varnothing 45\ \text{mm}$, both Schott Borofloat glass, $n_{635\ \text{nm}} = 1.46$) were mounted onto the aluminum housing shown in Fig. 5(a). To absorb the high power of the incident unscattered beam, a beam trap was attached to the measurement volume. In order to avoid reflections, the beam trap was not separated from the cylindrical cuvette, i.e., it was also filled with the investigated scattering medium. The incident beam was reflected in the beam trap under $30\ \text{deg}$ by a neutral density filter (OD 2.5). Hereby, only $\approx 0.5\%$ of the incident power was reflected, and the rest was absorbed in the filter. The reflected part was absorbed by the anodized wall. As particles with high anisotropy factor show significant forward scattering, the wall

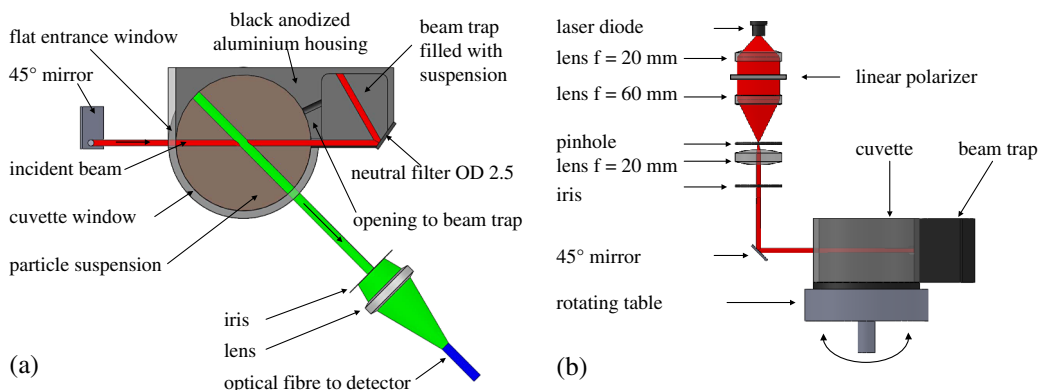


Fig. 5 (a) The cuvette and (b) the illumination setup for creating a collimated beam ($\varnothing = 2$ mm) for illumination of the cuvette. The illumination setup is fixed to the cuvette.

between the sample volume and the beam trap was removed between $\vartheta = 0$ deg and $\vartheta = -20$ deg. The forward scattered light, therefore, also entered the beam trap and was absorbed. The effect of using only a black tape with nonnegligible reflection for the absorbing layer was studied experimentally in Sec. 5.2.

Analogously to the simulation, the scattered light was detected by imaging the origin of the cuvette onto a $1000 \mu\text{m}$ optical fiber, using a 50 mm lens (200 mm distance to origin, 3 mm iris), see Fig. 5(a). The distal end of the optical fiber was faced to a silicon sensor (S2575, UDT Instruments, San Diego). The signal was amplified by a transimpedance amplifier (DDPCA-300, Femto Messtechnik GmbH, Berlin, Germany) with variable gain, and the resulting voltage signal was digitized by an A/D converter (RedLab 1608FS, Meilhaus Elektronik GmbH, Puchheim, Germany). The whole setup was computer controlled, automatically selecting the optimal gain of the transimpedance amplifier in each position, to keep the output voltage in the range of 0.05 V and 8 V . Thus, the optimal voltage range for the A/D converter was guaranteed, and the signal could be measured over ~ 7 orders of magnitude. For the measurements, we rotated the cuvette, including the illumination setup between $\vartheta = 0$ deg and $\vartheta = 180$ deg with a step size of 1 deg. In each position, 2000 measurement values were captured at a rate of 1 kHz and averaged with both the irradiated and the nonirradiated sample. The corresponding dark measurement was subtracted from each measurement of the irradiated sample. Before starting the detection process, the program stops for 500 ms after changing the illumination or the position for adjustment of the low-pass filter in the transimpedance amplifier. Therefore, one measurement from $\vartheta = 0$ deg to $\vartheta = 180$ deg takes about 10 min . The system was aligned by coupling an LED light source into the detector sided face of the optical fiber. The detection and the illumination volumes were then aligned by bringing the light spots to congruence. The cuvette was aligned by using the reflections from the surfaces.

4 Validation Measurements

In order to test the apparatus, we measured two different types of almost monodisperse microparticles. We used polystyrene spheres with a nominal diameter of $2.82 \mu\text{m}$ and SiO_2 particles with a nominal diameter of $4.40 \mu\text{m}$ (both: Forschungspartikel, Microparticles GmbH, Berlin, Germany). By the use of collimated transmission measurements and Mie theory, the diameter of the polystyrene spheres was determined

to be $2.752 \pm 0.020 \mu\text{m}$. For the SiO_2 particles, the nominal diameter of $4.40 \pm 0.25 \mu\text{m}$ was used. Both sphere suspensions were diluted with purified water (HiPerSolv, VWR, Fontenay-sous-Bois, France) to achieve a $\mu_s = 0.01 \text{ mm}^{-1}$. For each sphere size, three samples were prepared and measured. The averaged intensity for parallel polarization is shown in Fig. 6. For comparison, the phase functions based on Mie theory for the given diameters are also shown. The refractive index was assumed to be 1.586 for the polystyrene spheres²⁵ and 1.42 for the SiO_2 spheres (manufacturer information). The calculated anisotropy factor, using Mie theory, is $g = 0.856$ and $g = 0.989$ for the polystyrene and SiO_2 particles, respectively. Both measurements are in good agreement with the theory for the whole considered angular range from $\vartheta = 7$ deg to $\vartheta = 172$ deg. Similar results were obtained for the perpendicular polarization (data not shown). Even for the SiO_2 particles having an anisotropy factor close to 1 , no increase of the measured phase function for large angles can be seen. This proves that the absorbing layer is working fine. The measured raw data of the spheres were subtracted by a blank measurement of a cuvette filled with clear solvent (purified water). For all measurable angles, this background signal was at least 1 order of magnitude smaller than the signal of the spheres. These measurements show that we can directly obtain the

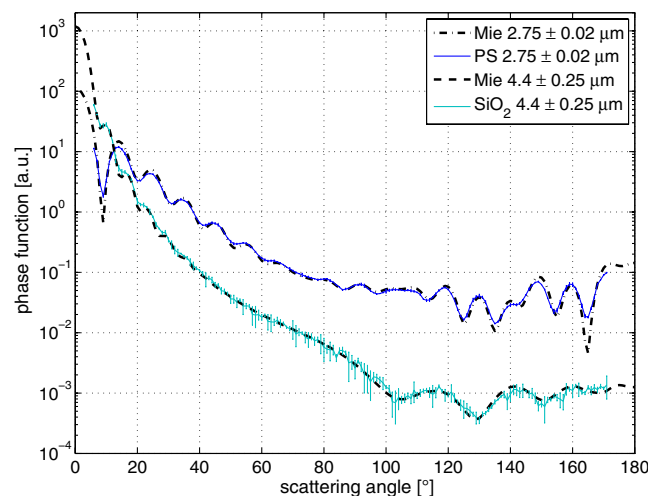


Fig. 6 Measured phase function (normalized to theory) for the two different spheres (polystyrene and SiO_2 , parallel polarization) in comparison with Mie theory calculations.

phase function of the spheres without any need for corrections when using the described goniometer. This is even true for the phase function of particles with a high anisotropy factor.

5 Applications

5.1 Fat Emulsions

A possible application of the presented apparatus is the measurement of the phase function of different fat emulsions like Intralipid 20%, commonly used as a scattering standard. A lot of work has been done to determine precisely the optical properties of Intralipid.^{26–28} However, the scattering phase function of these standards has been investigated poorly. Michels et al.²⁰ addressed this issue, but in contrast to the goniometer described in this paper, they used a plain cuvette without any absorbing layer. Thus, they had to correct the phase function for reflections by using the *a priori* information of the shape of the size distribution of the scatterers. Furthermore, angles around 90 deg were not measurable.

The results presented in Fig. 7 are the phase functions without any *a priori* information of the Intralipid 20%. For these measurements, the Intralipid 20% (Fresenius Kabi, Bad Homburg, Germany) was diluted with purified water, achieving a scattering coefficient of $\mu_s = 0.01 \text{ mm}^{-1}$. The dilution was based on the scattering coefficients of the pure products determined by Michels et al.²⁰ The phase function was measured for both polarizations, and the phase function representing unpolarized light was calculated by the arithmetic mean of both experiments. The error bars in Fig. 7 originate from three repetitions of the measurement. For each repetition the goniometer was newly adjusted before each measurement. In addition, the polarization state was changed after each repetition. The values of $p(\vartheta)$ at angles below $\vartheta = 7$ deg and above $\vartheta = 172$ deg were extrapolated, fitting the Henyey–Greenstein function and a second-order polynomial to the values of the adjacent 30 deg, respectively. The comparison of the two polarizations states shows large differences. For the parallel case, the phase function drops down for angles around 90 deg. This scattering feature resembles those of Rayleigh–Gans scatterers, indicating that Intralipid contains either a significant amount of scatterers

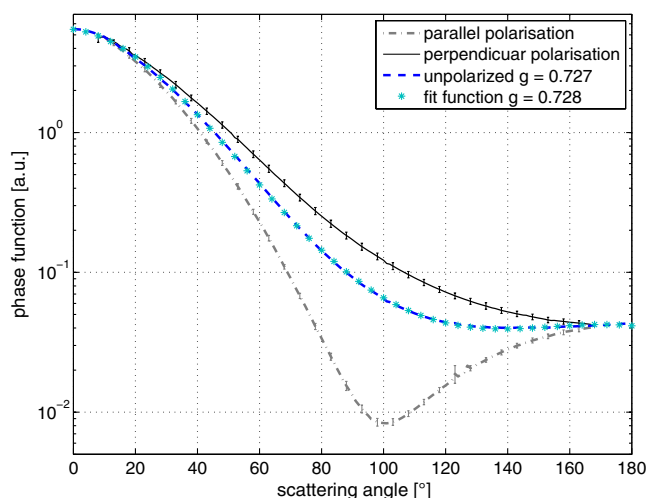


Fig. 7 Measured phase function for parallel and perpendicular incidence for Intralipid 20% and the calculated scattering phase function for the unpolarized case.

smaller than the wavelength, or larger scatterers with a refractive index close to the one of the surrounding medium. The phase function for unpolarized light decreases toward $\vartheta = 90$ deg and rises slightly again toward $\vartheta = 180$ deg. From this scattering phase function, the anisotropy factor g can be calculated using

$$g = \frac{\int_0^\pi p(\vartheta) \cos(\vartheta) \sin(\vartheta) d\vartheta}{\int_0^\pi p(\vartheta) \sin(\vartheta) d\vartheta}, \quad (2)$$

where $p(\vartheta)$ is the phase function. For Intralipid 20%, an anisotropy factor of $g = 0.727$ was obtained. This value is in good agreement to the anisotropy factor determined by measurements of μ_s (collimated transmission) and μ_s' (spatially resolved reflectance²⁹), resulting in a $g = 0.737$ at 635 nm.

For application of this phase function it is useful to describe it by an analytical function. The empirically determined function

$$\log_{10}[p(\vartheta)] = a + b\vartheta^2 + ce^{-d\vartheta} \cos(e\vartheta) \quad (3)$$

describes the phase function, using the parameters in Table 1 with an average error of $\approx 1.4\%$ (maximum error 4.2%). We also measured other fat emulsions of different concentration (all Fresenius Kabi, Bad Homburg, Germany). The results of the coefficients for Eq. (3) are also shown in Table 1. Even if the products look the same, the scattering phase function of the different brands varies considerably. Comparing the measured phase functions to the Henyey–Greenstein function with the same anisotropy factor, large differences can be obtained. For any applications of these phantom media, one should check carefully the influence of this difference. In contrast, two different containers of the same product Intralipid 20% (both Fresenius Kabi) bottled for Germany and Italy resulted in almost the same anisotropy factor ($g = 0.721$ and $g = 0.727$, respectively). The stability of the diluted Intralipid samples was checked by measuring the scattering phase function for parallel polarization of one sample periodically over 124 h. Before each measurement, the sample was carefully shaken. During this time period, almost no change in the scattering phase function could be observed.

The effect of unequal rising of lipid droplets of different sizes, caused by differences in the density between solvent and droplets, was found to be negligible. To study this issue, the phase function was measured in two steps (forward and

Table 1 Parameters for description of the scattering phase function of Intralipid 10% (IL10), Intralipid 20% (IL20), Intralipid 30% (IL30), and Lipovenoes 10% (LI10) at 662 nm.

Parameter	IL10	IL20	IL30	LI10
a	−0.06194	−0.1563	−0.2423	−0.2214
b	−0.07768	−0.1376	−0.1491	−0.1447
c	0.3805	0.8958	1.0952	1.0380
d	0.1124	0.1837	0.2222	0.1995
e	1.6845	1.585	1.5960	1.5792
g -factor	0.405	0.727	0.784	0.770
	± 0.002	± 0.002	± 0.003	± 0.001

backward scattering separately). Before each step, the sample was mixed carefully. Almost no deviation to the scattering phase function measured in one step could be found. Nevertheless, repetition measurements on one Intralipid sample during a whole day without mixing showed differences of the scattering phase between the first and the last measurement. Rising or sinking of particles has to be investigated for each sample material separately; especially, if the difference in density between particle and solvent is large.

5.2 Yeast Cells

In order to study a potential application, we measured yeast cells (Reinzuchtheffe Burgund, Hefereinzucht Schlag GmbH, Aalen, Germany) diluted with NaCl 0.9% solution. The scattering coefficient was again set to be $\mu_s \approx 0.01 \text{ mm}^{-1}$, using collimated transmission measurements. To show the importance of the novel setup, we also measured the yeast cells, using a round standard cuvette (692.103-BF $\varnothing = 45 \text{ mm}$, Hellma GmbH & Co. KG, Müllheim, Germany). The black absorbing layer was thereby realized by black tape. The total remission of the black tape was determined with an integrating sphere to be $\approx 5\%$. The scattering phase functions for both linear polarization states were measured with both cuvettes, and the unpolarized case was calculated by the arithmetic mean of both experiments. The phase function for the scattering angles below $\vartheta = 7 \text{ deg}$ and above $\vartheta = 172 \text{ deg}$ was extrapolated, using a third- and fifth-order polynomial, respectively, which was fitted to the scattering phase function of the adjacent 10 deg. The results of both setups are shown in Fig. 8. The scattering phase function for the parallel and the perpendicular case differ, especially for angles around $\vartheta = 90 \text{ deg}$. The scattering phase function for parallel polarization shows a minimum around $\vartheta = 90 \text{ deg}$. As there are no small oscillations visible, we conclude that the size of the yeast cells is not monodisperse. The scattering phase function measured with the standard cuvette shows an increase for angles toward $\vartheta = 180 \text{ deg}$, compared to the scattering phase function measured with the optimized cuvette. This can be explained by two effects. First, the incident beam is reflected by the surface of the tape and the photons more or less travel in the opposite direction. Second, the forward scattered light (note the anisotropy factor equals

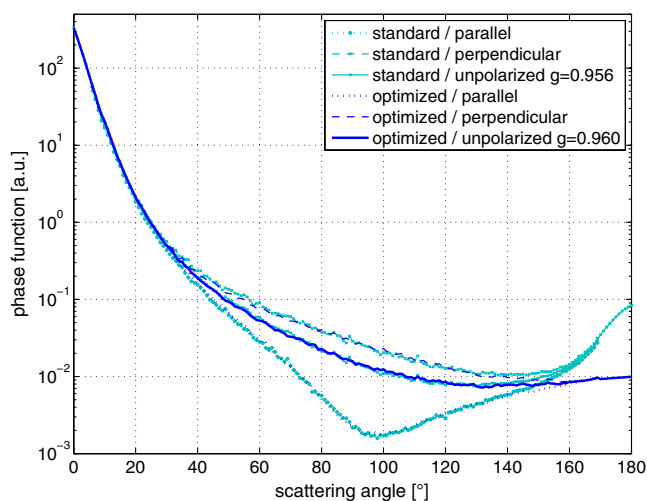


Fig. 8 Scattering phase function of yeast cells for different polarizations.

$g = 0.96$) is also reflected by the tape, and can enter the detector directly for detection angles larger than about $\vartheta = 140 \text{ deg}$. These measurements demonstrate the advantages of the improved goniometer. The determined anisotropy factor of the scattering phase function, measured with the standard and the optimized cuvette ($g = 0.956$ and $g = 0.960$, respectively), differs only slightly, as the huge forward scattering exceeds by far the backward scattered light. However, if the reduced scattering coefficient is calculated ($\mu'_s = \mu_s(1 - g)$), the difference between the two anisotropy factors causes an error of $\sim 10\%$ in μ'_s . The determined anisotropy factor of $g = 0.960$ is relatively high, but still in the range typically obtained for biological tissue.^{30,31}

6 Conclusion

In this work, we presented simulations and measurements of the phase function with an optimized goniometer. Validation measurements using polystyrene and SiO₂ spheres proved the concept of this apparatus. By use of the optimized goniometer, the scattering phase function of different fat emulsions like Intralipid could be determined. Furthermore, measurements of the scattering phase function of yeast cells illustrate the applicability of the goniometer for biological samples, and showed the improvement compared to a standard goniometer. For future application, the setup will be modified, using a white light source and a spectrometer for detection, in order to measure the scattering phase function for multiple wavelengths.

References

1. A. Ishimaru, *Wave Propagation and Scattering in Random Media*, Vol. 2, IEEE Press, Piscataway, NJ (1997).
2. F. Martelli et al., *Light Propagation Through Biological Tissue and Other Diffusive Media: Theory, Solutions, and Software*, SPIE Press, Bellingham (2010).
3. L. G. Henyey and J. L. Greenstein, "Diffuse radiation in the galaxy," *Astrophys. J.* **93**(1), 70–83 (1941).
4. G. Mie, "Beiträge zur Optik trüber Medien, speziell kolloidaler Metallösungen," *Ann. Phys.* **330**(3), 377–445 (1908).
5. S. C. Kanick et al., "Scattering phase function spectrum makes reflectance spectrum measured from intralipid phantoms and tissue sensitive to the device detection geometry," *Biomed. Opt. Express* **3**(5), 1086–1100 (2012).
6. J. P. Kratochvil and C. Smart, "Calibration of light-scattering instruments. III. Absolute angular intensity measurements on mie scatterers," *J. Colloid Sci.* **20**(8), 875–892 (1965).
7. S. Bantle, M. Schmidt, and W. Burchard, "Simultaneous static and dynamic light scattering," *Macromolecules* **15**(6), 1604–1609 (1982).
8. S. T. Flock, B. C. Wilson, and M. S. Patterson, "Total attenuation coefficients and scattering phase functions of tissues and phantom materials at 633 nm," *Med. Phys.* **14**(5), 835–841 (1987).
9. C. Braun and U. K. Krieger, "Two-dimensional angular light-scattering in aqueous nacl single aerosol particles during deliquescence and efflorescence," *Opt. Express* **8**(6), 314–321 (2001).
10. L. Zhao et al., "New versatile setup for goniometric measurements of spectral radiance," *Opt. Eng.* **45**(5), 053606 (2006).
11. J. L. Castagner and I. J. Bigio, "Polar nephelometer based on a rotational confocal imaging setup," *Appl. Opt.* **45**(10), 2232–2239 (2006).
12. K. Fu et al., "Polarized angular dependent light scattering properties of bare and pegylated gold nanoshells," *Curr. Nanosci.* **3**(2), 167–170 (2007).
13. Y. Zhu, Z. Ding, and M. Geiser, "Tissue scattering parameter estimation through scattering phase function measurements by goniometer," *Chin. Opt. Lett.* **5**(9), 531–533 (2007).
14. K. G. Privoznik, K. J. Daniel, and F. P. Incropera, "Absorption, extinction and phase function measurements for algal suspensions of chlorella

- pyrenoidosa," *J. Quant. Spectrosc. Radiat. Transfer* **20**(4), 345–352 (1978).
15. S. L. Jacques, C. A. Alter, and S. A. Prahl, "Angular dependence of HeNe laser light scattering by human dermis," *Lasers Life Sci.* **1**(4), 309–333 (1987).
 16. M. Firbank et al., "Measurement of the optical properties of the skull in the wavelength range 650–950 nm," *Phys. Med. Biol.* **38**(4), 503–510 (1993).
 17. R. Drezek, A. Dunn, and R. Richards-Kortum, "Light scattering from cells: finite-difference time-domain simulations and goniometric measurements," *Appl. Opt.* **38**(16), 3651–3661 (1999).
 18. D. Watson et al., "Elastic light scattering from single cells: orientational dynamics in optical trap," *Biophys. J.* **87**(2), 1298–1306 (2004).
 19. J. D. Wilson et al., "Light scattering from intact cells reports oxidative-stress-induced mitochondrial swelling," *Biophys. J.* **88**(4), 2929–2938 (2005).
 20. R. Michels, F. Foschum, and A. Kienle, "Optical properties of fat emulsions," *Opt. Express* **16**(8), 5907–5925 (2008).
 21. Ø. Svendsen et al., "Mueller matrix measurements of algae with different shape and size distributions," *Appl. Opt.* **50**(26), 5149–5157 (2011).
 22. J. R. Zijp and J. J. Ten Bosch, "Angular dependence of He–Ne-laser light scattering by bovine and human dentine," *Arch. Oral Biol.* **36**(4), 283–289 (1991).
 23. F. K. Forster et al., "Phase function measurements on nonspherical scatterers using a two-axis goniometer," *J. Biomed. Opt.* **11**(2), 024018 (2006).
 24. A. Liemert and A. Kienle, "Light transport in three-dimensional semi-infinite scattering media," *J. Opt. Soc. Am. A* **29**(7), 1475–1481 (2012).
 25. C. Tribastone and W. Peck, "Designing plastic optics: new applications emerging for optical glass substitutes," in *The Photonics Design and Applications Handbook*, L. Staff, Ed., pp. H426–H433, Laurin Publishing, Pittsfield, Massachusetts (1998).
 26. H. J. Van Staveren et al., "Light scattering in intralipid-10% in the wavelength range of 400–1100 nm," *Appl. Opt.* **30**(31), 4507–4514 (1991).
 27. F. Martelli and G. Zaccanti, "Calibration of scattering and absorption properties of a liquid diffusive medium at NIR wavelengths. CW method," *Opt. Express* **15**(2), 486–500 (2007).
 28. P. D. Ninni, F. Martelli, and G. Zaccanti, "Intralipid: towards a diffusive reference standard for optical tissue phantoms," *Phys. Med. Biol.* **56**(2), N21–N28 (2011).
 29. F. Foschum, M. Jäger, and A. Kienle, "Fully automated spatially resolved reflectance spectrometer for the determination of the absorption and scattering in turbid media," *Rev. Sci. Instrum.* **82**(10), 103104 (2011).
 30. W. F. Cheong, S. A. Prahl, and A. J. Welch, "A review of the optical properties of biological tissues," *IEEE J. Quantum Electron.* **26**(12), 2166–2185 (1990).
 31. M. Friebe et al., "Influence of oxygen saturation on the optical scattering properties of human red blood cells in the spectral range 250 to 2000 nm," *J. Biomed. Opt.* **14**(3), 034001–034001 (2009).